

Article

Experimental Damage Identification of a Model Reticulated Shell

Jing Xu ^{1,2}, Jiajia Hao ¹, Hongnan Li ^{2,3}, Minzhang Luo ^{4,*}, Wen Guo ¹ and Weijie Li ²

¹ School of Civil Engineering, Qingdao University of Technology, Qingdao 266033, China; jingxu180@qut.edu.cn (J.X.); haojiajs@hotmail.com (J.H.); gwen.ok@163.com (W.G.)

² Faculty of Infrastructure Engineering, Dalian University of Technology, Dalian 116024, China; hnli@dlut.edu.cn (H.L.); jack199008@gmail.com (W.L.)

³ School of Civil Engineering, Shenyang Jianzhu University, Shenyang 110168, China

⁴ Electronics and Information School, Yangtze University, Jingzhou 434023, China

* Correspondence: lmz@yangtzeu.edu.cn; Tel.: +86-716-8060-226

Academic Editor: Stefano Invernizzi

Received: 17 February 2017; Accepted: 29 March 2017; Published: 6 April 2017

Abstract: The damage identification of a reticulated shell is a challenging task, facing various difficulties, such as the large number of degrees of freedom (DOFs), the phenomenon of modal localization and transition, and low modeling accuracy. Based on structural vibration responses, the damage identification of a reticulated shell was studied. At first, the auto-regressive (AR) time series model was established based on the acceleration responses of the reticulated shell. According to the changes in the coefficients of the AR model between the damaged conditions and the undamaged condition, the damage of the reticulated shell can be detected. In addition, the damage sensitive factors were determined based on the coefficients of the AR model. With the damage sensitive factors as the inputs and the damage positions as the outputs, back-propagation neural networks (BPNNs) were then established and were trained using the Levenberg–Marquardt algorithm (L–M algorithm). The locations of the damages can be predicted by the back-propagation neural networks. At last, according to the experimental scheme of single-point excitation and multi-point responses, the impact experiments on a K6 shell model with a scale of 1/10 were conducted. The experimental results verified the efficiency of the proposed damage identification method based on the AR time series model and back-propagation neural networks. The proposed damage identification method can ensure the safety of the practical engineering to some extent.

Keywords: reticulated shell; damage detection; time series modeling; Levenberg–Marquardt algorithm; impact experiment; neural networks

1. Introduction

Long-span spatial structures are widely used in stadiums, theaters, exhibition centers, airport terminals, and many other large scale structures. Any one of these structures can simultaneously house a large number of occupants. As a result, guaranteeing the integrity of these structures is of great importance. Structural health monitoring (SHM) systems should be established for important buildings. For important buildings undergoing construction, a long-term health monitoring system should also be set up to monitor the health condition of the buildings during the construction and service stages. It is essential to monitor structural conditions and detect damage in real-time for future construction projects [1]. For structural health monitoring projects, one of the core approaches used is damage identification.

The study of SHM has attracted numerous interests in different fields of application. By using SHM technologies, the real-time damage detection of various structures, including concrete structures [2–6],

pipeline structures [7–12], and steel structures [13–19], can be investigated in order to provide early warning and hopefully to avoid accidents. In the aerospace industry, several application areas have garnered significant interests. Rapid inspection of satellite structures for pre-launch verification has been achieved using the SHM technologies [20–22].

Currently, damage identification based on the variation of modal parameters, such as resonant frequencies [23–25], mode shapes [26,27], mode shape curvatures [28,29], and modal strain energy [30–32], have been widely adopted. Most reticulated shell structure damage detection methods are also based on a variation of the modal parameters [33–37]. The methods based on modal parameters usually rely heavily on fast Fourier transform, which will cause bias errors. These errors will reduce the detection accuracy of the modal parameters. Since we can only acquire an incomplete set of modal parameters by experiments, we had to resort to methods of model reduction or modal shape expansion. These methods will lead to the loss of physical meaning of the damage factors. The damage identification of a reticulated shell has a number of associated difficulties due a large number of degrees of freedom (DOFs), the phenomenon of modal localization and transition, and low modeling accuracy. These characteristics will cause a problem in that the model parameters are not in the same order between the damaged conditions and the undamaged condition, which will further reduce the accuracy of the damage identification based on the variation of the modal parameters. In order to overcome the above difficulties, a damage identification method based on the vibration response of the structure can be adopted [38–40].

In this paper, a novel application of a damage detection method based on the time series model and back-propagation neural networks (BPNNs) using acceleration responses is developed. Firstly, the damage was identified by the auto-regressive (AR) time series model based on the changes in model coefficients. Secondly, the damage location was determined by the back-propagation neural networks in which the damage sensitive factors were used as inputs and the damage positions were used as outputs. Lastly, in order to verify the validity of this method, impact experiments of a K6 shell model with a 1/10 scale was conducted by using the scheme of single-point excitation and multi-point responses. Experimental results demonstrated the effectiveness of the proposed method in the damage identification of reticulated shell.

2. Methodologies

2.1. The Auto-Regressive Time Series Model

In a health monitoring system, a series of original acceleration data can be obtained from sensors placed on various locations of a structure with a certain sampling frequency. These data constitute the time series. The initial acceleration data should be pre-processed to remove the mean and the trend. After pre-processing, the acceleration time histories are compared to those time histories from different loading states (i.e., sizes, directions, and positions of loads) and different environmental cases. Assuming the signals before and after the damage are linear stationary, the AR model is established as follows:

$$X_t = \varphi_1 X_{t-1} + \varphi_2 X_{t-2} + \cdots + \varphi_p X_{t-p} + a_t \quad (1)$$

where X_t is the pre-processed acceleration signal, φ_i is the i th AR coefficients, p is the order of the AR model, and a_t is the residual term [38].

In Equation (1), the optimal model order is determined using the Akaike information criteria (AIC) and the AR coefficients are determined using the least squares method. Structural damages can cause changes to the acceleration responses, based on which the identification of damage can be achieved using the difference in AR model coefficients between the damage and the undamaged states of the structure. Using the first four AR coefficients, a damage-sensitive feature, DS_i is defined as follows:

$$DS_i = \varphi_{if} - \varphi_{id} \quad (2)$$

where DS_i is the i th damage-sensitive feature, φ_{if} and φ_{id} are the i th AR coefficients for damage and undamaged state, respectively. If the value of DS_i is zero, the structure is in the undamaged state. If not, the structure is in the damaged state.

2.2. Back-Propagation Neural Network

A neural network is a powerful tool of pattern classification and is suitable for the identification of the inherent characteristics before and after damage [41–44]. The traditional back-propagation neural network is a multi-layer feed-forward neural network, which consists of one input layer, one hidden layer, and one output layer, as shown in Figure 1.

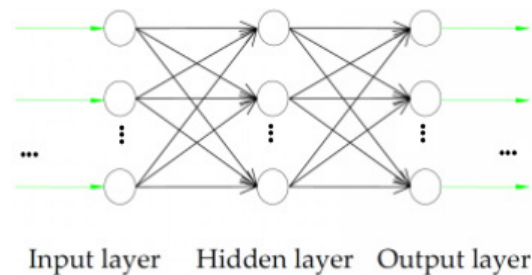


Figure 1. The architecture of a back-propagation neural networks (BPNNs).

If N_h is the numbers of nodes in the hidden layer, it can be calculated by the Formula (3) [45].

$$N_h \leq 4\sqrt{N_i(N_o + 3)} + 1 \quad (3)$$

where N_i is the number of nodes in the input layers and N_o is the number of nodes in the output layers.

The traditional back-propagation neural network employing the gradient descent algorithm can easily slow down the training process and fall into a local minimum. Here, we use the Levenberg–Marquardt algorithm (L–M algorithm), which is an improved training algorithm. It is a global optimization algorithm which computes and adjusts the connection weights according to the information from all samples. The L–M algorithm originated from the Newton optimization algorithm while integrating the gradient descent method, in order to reduce the computational complexity and accelerate the training rate of the network. The L–M algorithm is very suitable for solving the problems related to damage identification of spatial structures with large numbers of joints and bars.

2.3. Damage Detection Flowchart

Figure 2 illustrates the procedure of the proposed damage detection method, which is described as follows:

- (1) Measure the acceleration responses of the reticulated shell structure before and after damage under the excitation condition.
- (2) Obtain the stationary random acceleration signals by using the data pre-processed method introduced in Section 2.1.
- (3) Establish the auto-regressive time series model (AR model) by using the modeling method introduced in Section 2.1.
- (4) Detect the damage of the reticulated shell according to the changes in the coefficients of the AR model before and after damage.
- (5) Obtain the damage sensitive factors by using Equation (2).
- (6) Train the back-propagation neural networks (BPNNs) by using the method introduced in Section 2.2, with the damage sensitive factors as the inputs and the damage positions as the outputs.

- (7) Find the locations of the damages by testing the trained BPNNs.

This paper develops the novel application of a damage detection method based on the time series AR model and BPNNs using acceleration responses of the reticulated shell. This method has the advantages of relaxing the requirement of prior knowledge about the excitation input and the modal parameters. It effectively eliminates the method’s dependency on modeling accuracy and improves the damage detection accuracy for a reticulated shell.

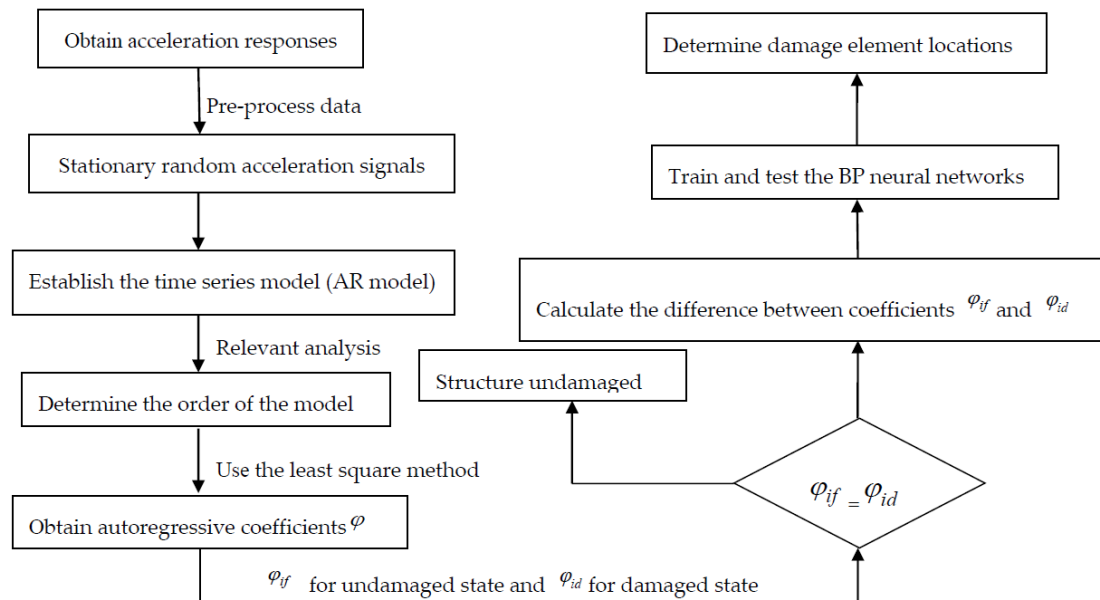


Figure 2. Flowchart of the proposed damage detection method.

3. Experimental Setup

Impact experiments on a K6 shell model with a scale of 1/10 were conducted in order to verify the efficiency of this damage identification method based on the time series model and the improved BPNNs. The proposed damage identification method can serve as a reference for practical engineering.

3.1. Experiment Model

As shown in Figure 3, a K6 single-layer spherical shell (span × height: 3 m × 0.5 m) with a scale of 1/10 was constructed. The shell was composed of 90 seamless steel tubes (Φ13 × 2). We simulated the roof load by attaching solid steel balls. These solid steel balls were all the same size, each with the diameter of 150 mm and the weight of 13.2 kg. There were 19 steel balls in total. The material properties of the experimental model are shown in Table 1 and the lengths of the bar elements are shown in Table 2. According to the principle of equivalent stiffness, we simulated the structural damage by replacing certain bar elements with smaller sized elements. The cross-section of the replacement elements and their corresponding damage degrees are shown in Table 3. The replacement elements and the model were bolted through the end plate, as shown in Figure 4. The model base was composed of 18 welded square steel tubes (100 mm × 200 mm × 4 mm) and 18 ball joints at the outer ring of the reticulated shell were connected to the base. The base was firmly connected to the ground by the anchor bolt.



Figure 3. Photo of test model of the K6 single-layer spherical shell.



Figure 4. Connection between the model and replacement element.

Table 1. Material characteristics of experimental model.

| Grade of Steel | Elastic Modulus E (N/m ²) | Steel Density (kg/m ³) | Poisson's Ratio |
|----------------|---------------------------------------|------------------------------------|-----------------|
| Q235 | 2.07×10^{11} | 7800 | 0.3 |

Table 2. The lengths of the bar elements (mm).

| Main Rib Elements | First Ring Elements | Second Radial Elements | Second Ring Elements | Third Radial Elements-1 | Third Radial Elements-2 | Third Ring Elements |
|-------------------|---------------------|------------------------|----------------------|-------------------------|-------------------------|---------------------|
| 35.2 | 532.1 | 659.4 | 538.3 | 577.8 | 688.9 | 520.9 |

Table 3. The cross-section of the replacement elements and their corresponding damage degrees.

| Damaged Degree | 0 | 40% | 50% | 60% | 70% | 80% |
|----------------|--------------------|--------------------|--------------------|-------------------|-------------------|-------------------|
| Cross-section | $\Phi 13 \times 2$ | $\Phi 10 \times 3$ | $\Phi 10 \times 2$ | $\Phi 9 \times 2$ | $\Phi 8 \times 2$ | $\Phi 7 \times 2$ |

3.2. Experimental Scheme

Based on the experimental scheme for single-point excitation and multi-point responses, a single vertical downward point excitation on the top joint of the lattice shell model was excited by an impact hammer in order to get the acceleration response. The top joint of the lattice shell model had the largest vibration amplitude during the testing. Thus, the acceleration signal from the top joint had the best signal to noise ratio.

Since the number of sensors is limited in practical health monitoring projects and the number of shell nodes is large, we placed the sensors based on the particle swarm optimization algorithm (PSO) in this experiment. Particle swarm optimization was inspired by the simulation of a simplified social mode for a group of birds, firstly proposed by Kennedy in 1995 [46]. The method has characteristics of ease of implementation, high quality of solutions, computational efficiency, and speed of convergence [47]. For the optimization of the sensors, the fitness function can be defined based on bending deformation energy. Minimization values calculated based on the fitness function were desired in the optimization

procession. Though comparing the evaluation of a particle’s previous best value and the group’s previous best, the velocities and positions of particles were updated until the optimal positions were found. The optimal sensor positions, as shown in Figure 5, can be obtained for a given sensor number. The effects of the number and locations of the sensors were studied by the authors to some extent in [48]. Under the condition of a given sensor’s location, the damage detection accuracy can be improved with an increase in the number of sensors.

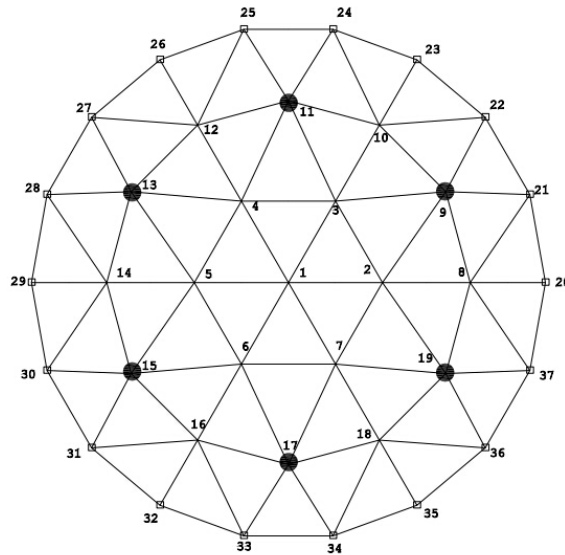


Figure 5. The optimal sensor placement positions.

The accelerometers were attached to the model firmly using strong magnets. The accelerometer used was the ICP accelerometer (model INV9822, China Orient Institute of Noise & Vibration, Beijing, China), which was manufactured by Beijing Orient Institute of Noise & Vibration. The hammer used was an MSC-3 impact hammer and the data acquisition instrument was a 24-bit high precision USB data acquisition instrument (model INV3018A). The instrumentation of the impact experiments is shown in Figure 6.

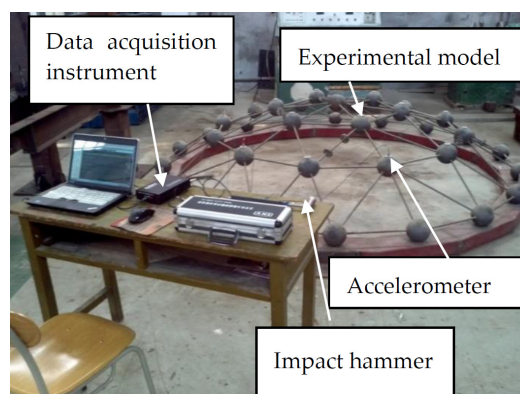


Figure 6. Instrumentation for impact experiments.

As a reticulated shell has a large number of degrees of freedom (DOFs), smaller damage levels of the elements can only affect the structural stiffness matrix slightly. Thus, smaller damage levels to an individual element have a relatively-low effect on the whole structure bearing capacity. On the other hand, due to various inevitable errors in the experiment, slight variations of test signals caused by the smaller damage levels of an individual element may be hidden by different kinds of random

errors, such as model errors and measurement errors. Therefore, we set damage levels between 40% and 80% in the experiment, as shown in Table 4. A higher level of damage to an individual element will increase the nonlinear influence on the structural vibration, which will cause instability failure more quickly. Instability failure is one of the most important causes for a reticulated shell to collapse.

Table 4. The damage and undamaged conditions.

| Condition | Damage Element Number and Damage Degree | Specifications of Replacements |
|--|---|--------------------------------|
| Undamaged condition | GK1 No damage | $\Phi 13 \times 2$ (undamaged) |
| Double component damage training condition | GK2 No. 8 and 38: 50% damage | $\Phi 10 \times 2$ |
| | GK3 No. 8 and 67: 50% damage | $\Phi 10 \times 2$ |
| | GK4 No. 22 and 38: 50% damage | $\Phi 10 \times 2$ |
| | GK5 No. 22 and 67: 50% damage | $\Phi 10 \times 2$ |
| | GK6 No. 38 and 67: 50% damage | $\Phi 10 \times 2$ |
| Double component damage experiment condition | GK7 No. 8 and 67: 40% damage | $\Phi 10 \times 3$ |
| | GK8 No. 22 and 38: 60% damage | $\Phi 9 \times 2$ |
| | GK9 No. 22 and 67: 70% damage | $\Phi 8 \times 2$ |
| | GK10 No. 38 and 67: 80% damage | $\Phi 7 \times 2$ |

The codes of the bar elements are shown in Figure 7. We can obtain acceleration responses of the six optimal node locations for the damaged conditions and undamaged condition. Take Node 9 as an example, the acceleration response of Node 9 for GK9 condition is shown in Figure 8.

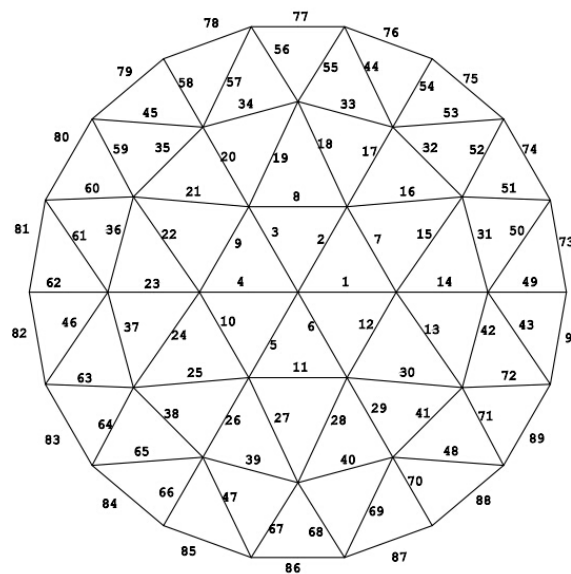


Figure 7. The codes of the elements.

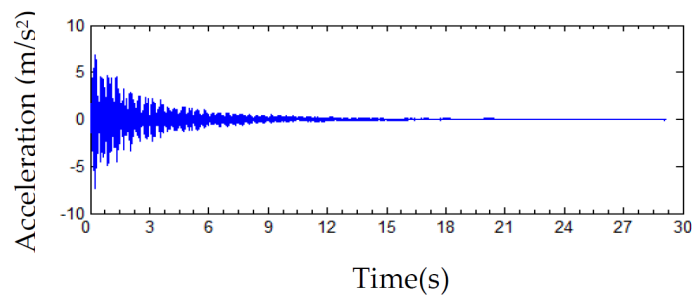


Figure 8. Acceleration responses of Node 9 for GK9.

4. Experimental Results

From the impact experiments on the single layer shell model, we obtained the acceleration responses of six nodes under different damage conditions. The sampling frequency was 500 Hz and the recording duration was 20 s. The 10,000 data points from the 5th second to the 25th second were chosen. In order to check the robustness of the method, 3% noise was added to the acceleration signal to build the AR model. Taking GK7, GK8, GK9, and GK10 as examples, a comparison of the first four coefficients of the constructed AR model between the undamaged condition and damaged condition is shown in Table 5. As we can see from Table 5, compared with the undamaged condition GK1, the AR model coefficients φ_i were changed under the damaged condition of GK7, GK8, GK9, and GK10, which indicates that damage has occurred.

Table 5. A comparison of auto-regressive (AR) model coefficients between the undamaged condition and damaged condition.

| Number of the Nodes | | Undamaged Condition | | Damaged Condition | | |
|---------------------|-------------|---------------------|--------|-------------------|--------|--------|
| | | GK1 | GK7 | GK8 | GK9 | GK10 |
| Node 9 | φ_1 | -3.08 | -3.165 | -3.496 | -3.708 | -3.209 |
| | φ_2 | 5.627 | 5.403 | 6.802 | 7.637 | 5.378 |
| | φ_3 | -9.294 | -7.658 | -11.09 | -13.14 | -7.433 |
| | φ_4 | 13.99 | 10.25 | 16.61 | 20.9 | 9.613 |
| Node 11 | φ_1 | -3.074 | -3.403 | -3.174 | -3.21 | -3.391 |
| | φ_2 | 5.509 | 6.362 | 5.772 | 6.006 | 6.323 |
| | φ_3 | -8.796 | -9.887 | -9.19 | -9.806 | -9.857 |
| | φ_4 | 13.18 | 14.35 | 13.78 | 15.15 | 14.45 |
| Node 13 | φ_1 | -3.191 | -3.627 | -3.168 | -3.456 | -3.038 |
| | φ_2 | 6.135 | 7.446 | 5.186 | 6.485 | 4.658 |
| | φ_3 | -10.76 | -12.9 | -7.004 | -10.11 | -6.053 |
| | φ_4 | 17.28 | 20.78 | 9.16 | 14.99 | 8.029 |
| Node 15 | φ_1 | -3.05 | -3.384 | -2.986 | -2.927 | -2.992 |
| | φ_2 | 5.534 | 6.198 | 4.536 | 4.618 | 4.745 |
| | φ_3 | -8.938 | -9.564 | -5.832 | -6.559 | -6.477 |
| | φ_4 | 13.35 | 13.87 | 7.439 | 9.219 | 8.446 |
| Node 17 | φ_1 | -3.37 | -3.296 | -3.077 | -2.928 | -3.154 |
| | φ_2 | 6.882 | 6 | 5.252 | 5.029 | 5.507 |
| | φ_3 | -11.91 | -9.375 | -7.925 | -7.84 | -8.37 |
| | φ_4 | 18.52 | 13.65 | 11.41 | 11.29 | 11.99 |
| Node 19 | φ_1 | -2.939 | -3.336 | -3.517 | -3.587 | -2.883 |
| | φ_2 | 5.223 | 6.047 | 7.164 | 7.271 | 4.454 |
| | φ_3 | -8.489 | -9.355 | -12.67 | -12.58 | -6.095 |
| | φ_4 | 12.83 | 13.64 | 20.85 | 20.3 | 8.032 |

Damage factors DS_i for the damaged conditions and the undamaged condition damage were calculated according to Equation (2). Based on the training conditions in Table 4, the network sample database was constructed. The structure of the BPNNs was set as 24 input nodes, 70 hidden nodes, and 5 output nodes. The maximum training times was 500. The training accuracy was 10^{-10} , and the learning factor was $\eta = 0.01$. The momentum coefficient was $\alpha = 0.9$ and the transfer function was the logarithmic sigmoid function. The neural networks were able to be established based on the L–M algorithm. After training, the neural networks were able to map any nonlinear relationships between the inputs and the outputs [49]. Then the experimental results were inputted into the BNPP model to identify the damage locations. The training conditions and experiment conditions are shown in Table 4. The network training process is shown in Figure 8 and the results of the network experiment are shown in Table 6. From Table 6, we can conclude that the damage identification method based on the time series model and L–M algorithm for a long-span spatial shell structure can accurately identify the damage locations. It can be proven that this method is accurate, feasible, and has a certain degree of anti-noise ability.

In Figure 9, we can conclude that the network training process based on L–M algorithm realizes convergence very quickly. To further illustrate the effectiveness of the L–M algorithm, the training process based on traditional training algorithm is shown in Figure 10, which shows that the convergence speed of the network training process based on the traditional algorithm is very slow. The damage conditions for the two different training algorithms are the same. These results further verify the effectiveness of the proposed damage identification method.

Table 6. The prediction result of networks when two elements are damaged (the target result of networks in the parenthesis).

| Element Number | GK7 | GK8 | GK9 | GK10 |
|----------------|----------------------------|---------------------------|---------------------------|----------------------------|
| No. 8 and 38 | 6.51×10^{-15} (0) | 1.93×10^{-7} (0) | 3.54×10^{-8} (0) | 6.67×10^{-10} (0) |
| No. 8 and 67 | 1(1) | 2.25×10^{-8} (0) | 4.04×10^{-8} (0) | 3.54×10^{-8} (0) |
| No. 22 and 38 | 3.4×10^{-9} (0) | 1(1) | 2.96×10^{-4} (0) | 8.55×10^{-4} (0) |
| No. 22 and 67 | 2.45×10^{-6} (0) | 2.64×10^{-7} (0) | 1(1) | 1.1×10^{-7} (0) |
| No. 38 and 67 | 7.21×10^{-8} (0) | 1.59×10^{-7} (0) | 4.77×10^{-8} (0) | 1(1) |
| results | true | true | true | true |

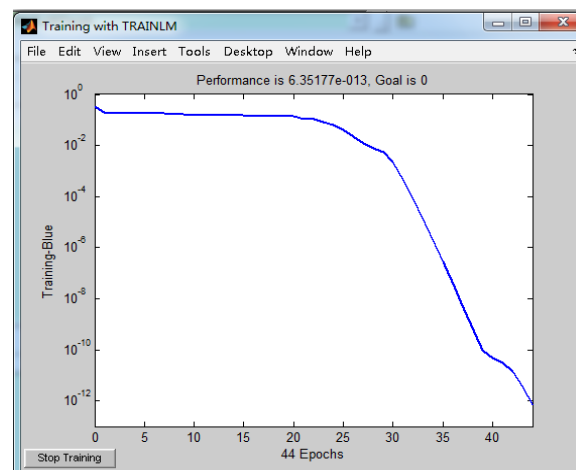


Figure 9. The training process based on the Levenberg–Marquardt (L–M) algorithm.

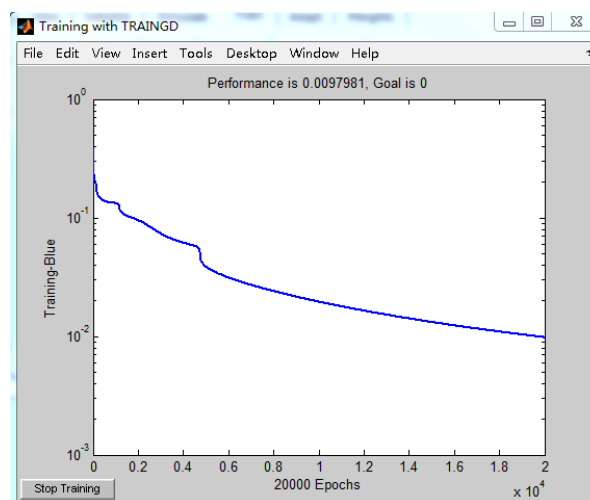


Figure 10. The training process based on the traditional algorithm.

5. Conclusions

For the damage identification of a reticulated structure, the proposed damage identification method based on the AR model and the L–M algorithm was verified by experiments on a model structure. The major conclusions of the study are summarized as follows:

- (1) The AR model was established based directly on the acceleration responses of the nodes. Using the coefficients of the AR model, the damage sensitive features were defined. Taking the damage sensitive features as the inputs and the damage locations as the outputs, an improved back-propagation neural network was established based on the L–M algorithm. The trained network can be used to detect the damage location of a reticulated shell. The proposed damage detection method does not require modal parameter identification and excitation information. It improves the accuracy of damage identification to some extent.
- (2) According to the principle of equivalent stiffness, we simulated the structural damage by replacing cross-sectional elements with smaller sized elements. The experiment scheme of single-point excitation and multi-point responses was adopted. Then, we conducted impact experiments on a K6 single-layer spherical shell with a scale of 1/10. The experimental results showed that the damage detection method based on the AR model and the L–M algorithm improved back-propagation neural network accurately identified the damage and the location of the damage that occurred in the reticulated shell.
- (3) Accuracy of the damage identification method is influenced by some factors, such as the sensor placement, neural network structure, and training algorithm of the neural network. In this paper, the sensor placement was optimized based on the particle swarm optimization algorithm.
- (4) The L–M algorithm was used to train the back-propagation neural network, which has the characteristics of faster training speed and better local searching ability. In addition, the accuracy of damage identification is effectively improved.

Acknowledgments: This research was supported by the National Natural Science Foundation of China (Project No. 51068019), the Provincial Natural Science Foundation of Shandong (Project No. ZR2013EEL013), the Provincial Natural Science Foundation of Hubei (Project No. 2013CFB399), and the International Cooperation Program for Excellent Lectures funded by the Shandong Provincial Education Department.

Author Contributions: Jing Xu designed the experiment and wrote part of the paper; Jiajia Hao and Wen Guo conducted the experiment and analyzed the data; Hongnan Li conceived the idea; Mingzhang Luo wrote part of the paper and proofread the entire paper; Weijie Li wrote the paper and offered critical comments.

Conflicts of Interest: The authors declare no conflict of interest.

References

1. Li, H.-N. Safety assessment, health monitoring and damage diagnosis for structures in civil engineering. *Earthq. Eng. Eng. Vib.* **2002**, *22*, 82–90.
2. Kong, Q.; Feng, Q.; Song, G. Water presence detection in a concrete crack using smart aggregates. *Int. J. Smart Nano Mater.* **2015**, *6*, 149–161. [[CrossRef](#)]
3. Siu, S.; Ji, Q.; Wu, W.; Song, G.; Ding, Z. Stress wave communication in concrete: I. Characterization of a smart aggregate based concrete channel. *Smart Mater. Struct.* **2014**, *23*, 125030. [[CrossRef](#)]
4. Kong, Q.; Hou, S.; Ji, Q.; Mo, Y.; Song, G. Very early age concrete hydration characterization monitoring using piezoceramic based smart aggregates. *Smart Mater. Struct.* **2013**, *22*, 085025. [[CrossRef](#)]
5. Ho, S.C.M.; Ren, L.; Li, H.-N.; Song, G. A fiber bragg grating sensor for detection of liquid water in concrete structures. *Smart Mater. Struct.* **2013**, *22*, 055012. [[CrossRef](#)]
6. Kong, Q.; Robert, R.H.; Silva, P.; Mo, Y. Cyclic crack monitoring of a reinforced concrete column under simulated pseudo-dynamic loading using piezoceramic-based smart aggregates. *Appl. Sci.* **2016**, *6*, 341. [[CrossRef](#)]
7. Zhao, X.; Li, W.; Zhou, L.; Song, G.; Ba, Q.; Ho, S.C.M.; Ou, J. Application of support vector machine for pattern classification of active thermometry-based pipeline scour monitoring. *Struct. Control Health Monit.* **2015**, *22*, 903–918. [[CrossRef](#)]

8. Hou, Q.; Jiao, W.; Ren, L.; Cao, H.; Song, G. Experimental study of leakage detection of natural gas pipeline using FBG based strain sensor and least square support vector machine. *J. Loss Prev. Process Ind.* **2014**, *32*, 144–151. [[CrossRef](#)]
9. Feng, Q.; Kong, Q.; Huo, L.; Song, G. Crack detection and leakage monitoring on reinforced concrete pipe. *Smart Mater. Struct.* **2015**, *24*, 115020. [[CrossRef](#)]
10. Jia, Z.G.; Ren, L.; Li, H.N.; Ho, S.C.; Song, G.B. Experimental study of pipeline leak detection based on hoop strain measurement. *Struct. Control Health Monit.* **2015**, *22*, 799–812. [[CrossRef](#)]
11. Ren, L.; Jia, Z.-G.; Li, H.-N.; Song, G. Design and experimental study on FBG hoop-strain sensor in pipeline monitoring. *Opt. Fiber Technol.* **2014**, *20*, 15–23. [[CrossRef](#)]
12. Du, G.; Kong, Q.; Lai, T.; Song, G. Feasibility study on crack detection of pipelines using piezoceramic transducers. *Int. J. Distrib. Sens. Netw.* **2013**. [[CrossRef](#)]
13. Yao, P.; Kong, Q.; Xu, K.; Jiang, T.; Huo, L.-S.; Song, G. Structural health monitoring of multi-spot welded joints using a lead zirconate titanate based active sensing approach. *Smart Mater. Struct.* **2015**, *25*, 015031. [[CrossRef](#)]
14. Ruan, J.; Zhang, Z.; Wang, T.; Li, Y.; Song, G. An anti-noise real-time cross-correlation method for bolted joint monitoring using piezoceramic transducers. *Smart Struct. Syst.* **2015**, *16*, 281–294. [[CrossRef](#)]
15. Yin, H.; Wang, T.; Yang, D.; Liu, S.; Shao, J.; Li, Y. A smart washer for bolt looseness monitoring based on piezoelectric active sensing method. *Appl. Sci.* **2016**, *6*, 320. [[CrossRef](#)]
16. Shao, J.; Wang, T.; Yin, H.; Yang, D.; Li, Y. Bolt looseness detection based on piezoelectric impedance frequency shift. *Appl. Sci.* **2016**, *6*, 298. [[CrossRef](#)]
17. Feng, D.; Feng, M.Q. Vision-based multipoint displacement measurement for structural health monitoring. *Struct. Control Health Monit.* **2015**. [[CrossRef](#)]
18. Feng, D.; Feng, M.Q. Experimental validation of cost-effective vision-based structural health monitoring. *Mech. Syst. Signal Process.* **2017**, *88*, 199–211. [[CrossRef](#)]
19. Feng, D.; Feng, M.Q. Output-only damage detection using vehicle-induced displacement response and mode shape curvature index. *Struct. Control Health Monit.* **2016**. [[CrossRef](#)]
20. Zagrai, A.; Doyle, D.; Arritt, B. Embedded nonlinear ultrasonics for structural health monitoring of satellite joints. In Proceedings of the 15th International Symposium on: Smart Structures and Materials & Nondestructive Evaluation and Health Monitoring, San Diego, CA, USA, 9 March 2008.
21. Yi, C.; Lv, Y.; Dang, Z.; Xiao, H. A novel mechanical fault diagnosis scheme based on the convex 1-D second-order total variation denoising algorithm. *Appl. Sci.* **2016**, *6*, 403. [[CrossRef](#)]
22. Mao, Z.; Todd, M. A structural transmissibility measurements-based approach for system damage detection. In Proceedings of the SPIE Smart Structures and Materials + Nondestructive Evaluation and Health Monitoring, San Diego, CA, USA, 9 March 2010.
23. Żak, A.; Krawczuk, M.; Ostachowicz, W. Vibration of a laminated composite plate with closing delamination. *J. Intell. Mater. Syst. Struct.* **2001**, *12*, 545–551. [[CrossRef](#)]
24. Mroz, Z.; Lekszycki, T. Identification of damage in structures using parameter dependent modal response. In Proceedings of the International Seminar on Modal Analysis, Leuven, Belgium, 10–12 September 1998; pp. 121–126.
25. Todd, M.; Johnson, G.; Vohra, S. Progress towards deployment of bragg grating-based fiber optic systems in structural monitoring applications. In Proceedings of the European COST F3 Conference on System Identification and Structural Health Monitoring, Madrid, Spain, 6–9 June 2000; pp. 521–530.
26. Natke, H.; Cempel, C. Model-aided diagnosis based on symptoms. In Proceedings of the DAMAS, Sheffield, UK, 30 June–2 July 1997; pp. 363–375.
27. Strubbs, N.; Sikorsky, C.; Park, S.; Bolton, R. *Verification of a Methodology to Nondestructively Evaluate the Structural Properties of Bridges*; Structural Health Monitoring Workshop, Stanford Univ.: Palo Alto, CA, USA, 1999; pp. 440–449.
28. Maeck, J.; Wahab, M.A.; Peeters, B.; De Roeck, G.; De Visscher, J.; De Wilde, W.; Ndambi, J.-M.; Vantomme, J. Damage identification in reinforced concrete structures by dynamic stiffness determination. *Eng. Struct.* **2000**, *22*, 1339–1349. [[CrossRef](#)]
29. Wang, M.L.; Xu, F.L.; Lloyd, G.M. Systematic numerical analysis of the damage index method used for bridge diagnostics. In Proceedings of the SPIE's 7th Annual International Symposium on Smart Structures and Materials, Newport Beach, CA, USA, 6 March 2000; pp. 154–164.

30. Zhang, L.; Quiong, W.; Link, M. A structural damage identification approach based on element modal strain energy. In Proceedings of the ISMA23, Noise and Vibration Engineering, Leuven, Belgium, 16–18 September 1998.
31. Worden, K.; Manson, G.; Fieller, N.R. Damage detection using outlier analysis. *J. Sound Vib.* **2000**, *229*, 647–667. [[CrossRef](#)]
32. Carrasco, C.J.; Osegueda, R.A.; Ferregut, C.M.; Grygier, M. Localization and quantification of damage in a space truss model using modal strain energy. In Proceedings of the Smart Structures and Materials 1997, San Diego, CA, USA, 23 May 1997; pp. 181–192.
33. Zhuo, W. Validity analysis on curvature modal method for damage localization to reticulated shell structures. *Sichuan Build. Sci.* **2012**, *3*, 024.
34. Liu, F.-L.; Yan, W.-M.; He, H.-X.; Wang, Z. Mode shape characterization and damage detection in latticed shell structures based on zernike moments. *Eng. Mech.* **2013**, *8*, 003.
35. Lu, W.; Teng, J.; Xu, Y.; Su, Z. Identification of damage in dome-like structures using hybrid sensor measurements and artificial neural networks. *Smart Mater. Struct.* **2013**, *22*, 105014. [[CrossRef](#)]
36. Wang, M.H.; Ji, C.M.; Luo, S.S. Research on structural damage identification of reticulated shell based on change rate of modal strain energy and wavelet analysis. *Appl. Mech. Mater.* **2014**, *578–579*, 296–300. [[CrossRef](#)]
37. Wang, M.; Dong, S.; Ji, C.; Yang, X. Research on damage identification of grid structures based on frequency response function, energy, environment and green building materials. In Proceedings of the 2014 International Conference on Energy, Environment and Green Building Materials (EEGBM 2014), Guilin, China, 28–30 November 2014; CRC Press: Guilin, China, 2015; p. 399.
38. Nair, K.K.; Kiremidjian, A.S.; Law, K.H. Time series-based damage detection and localization algorithm with application to the asce benchmark structure. *J. Sound Vib.* **2006**, *291*, 349–368. [[CrossRef](#)]
39. Krishnan Nair, K.; Kiremidjian, A.S. Time series based structural damage detection algorithm using gaussian mixtures modeling. *J. Dyn. Syst. Meas. Control* **2007**, *129*, 285–293. [[CrossRef](#)]
40. Noh, H.Y.; Nair, K.K.; Kiremidjian, A.S.; Loh, C. Application of time series based damage detection algorithms to the benchmark experiment at the national center for research on earthquake engineering (NCREE) in taipei, taiwan. *Smart Struct. Syst.* **2009**, *5*, 95–117. [[CrossRef](#)]
41. Carneiro, L.; Foti, D.; Ivorra, S. On modeling an innovative monitoring network for protecting and managing cultural heritage from risk events. *Key Eng. Mater.* **2014**, *628*, 243–249. [[CrossRef](#)]
42. Carneiro, L.; Nitti, R. A NN-based approach for monitoring early warnings of risk in historic buildings via image novelty detection. *Key Eng. Mater.* **2014**, *628*, 212–217. [[CrossRef](#)]
43. Carneiro, L.; Foti, D.; Vacca, V. On damage monitoring in historical buildings via neural networks. In Proceedings of the Environmental, Energy and Structural Monitoring Systems (EESMS), Trento, Italy, 9–10 July 2015; IEEE Workshop: Trento, Italy; pp. 157–161.
44. Ivorra, S.; Brotóns, V.; Foti, D.; Diaferio, M. A preliminary approach of dynamic identification of slender buildings by neuronal networks. *Int. J. Non-Linear Mech.* **2016**, *80*, 183–189. [[CrossRef](#)]
45. Chang, C.; Chang, T.; Xu, Y.; Wang, M. Structural damage detection using an iterative neural network. *J. Intell. Mater. Syst. Struct.* **2000**, *11*, 32–42. [[CrossRef](#)]
46. Kennedy, J. Particle swarm optimization. In *Encyclopedia of Machine Learning*; Springer: New York, NY, USA, 2011; pp. 760–766.
47. Kulkarni, R.V.; Venayagamoorthy, G.K. Particle swarm optimization in wireless-sensor networks: A brief survey. *IEEE Trans. Syst. Man Cybern. C (Appl. Rev.)* **2011**, *41*, 262–267. [[CrossRef](#)]
48. Xu, J.; Li, Z.; Diao, Y.-S. Optimal placement of strain sensors for monitoring systems on reticulated shells using particle swarm optimization. *Progress Steel Build. Struct.* **2013**, *1*, 017.
49. Lv, J.; Ren, H.; Gao, K. Artificial neural network-based constitutive relationship of inconel 718 superalloy construction and its application in accuracy improvement of numerical simulation. *Appl. Sci.* **2017**, *7*, 124. [[CrossRef](#)]

